# NUMERICAL AND EXPERIMENTAL STUDY FOR THE IDENTIFICATION OF DEFECTS IN WIND TRUBINE BLADES BY INFRARED THERMOGRAPHY

**Barthélemy Topilko[1,2], Ziad Salloum[1], Benjamin Méthot[1], Humberto Loaiza-Correa[3], Andrés David Restrepo[3], Xavier P. V. Maldague[1*]**

[1] Université Laval, Québec, Canada. E-mail: barthelemy.topilko.1@ulaval.ca, ziad.salloum.1@ulaval.ca, benjamin.methot.1@ulaval.ca, xavier.maldague@gel.ulaval.ca

[2] Université du Québec à Rimouski (UQAR), Rimouski, Canada Email: barthelemy.topilko@uqar.ca

[3] Escuela de Ingeniería Eléctrica y Electrónica, Facultad de Ingeniería, Universidad del Valle, Cali-Colombia.

E-mail: humberto.loaiza@correounivalle.edu.co, andres.david.restrepo@correounivalle.edu.co, https://eiee.univalle.edu.co/humberto-loaiza-correa

**Key Words:** Infrared thermography, active thermography, passive thermography, defect detection, wind energy, FEM

**Abstract.** Research in the field of renewable energies is today a major axis in the fight against global warming. Among these, wind energy appears to be a growing alternative in several territories around the world. During their use, inclusions and defects in the blades of wind turbines appear. It is the responsibility of the operator to perform periodic maintenance and inspections to maintain the quality of the installations. The objective of this project is to propose an industrial inspection vision method that allows the visualization of defects within a wind turbine blade using thermography methods. Currently, these techniques are already widely used in many different fields, such as the inspection of helicopter blades in the aeronautics field. It is necessary to have a temperature gradient within the object to be examined to have a contrast highlighting the defective areas of the blade. For the inspection of wind turbines, if the meteorological situation allows it, the sun will play the role of heat source heating the wind turbine blades in a real situation, in a passive thermographic approach. Our work is divided into three distinct parts. First, a simplified model of a wind turbine blade was modeled with the COMSOL Multiphysics software. Second, a sample with defects like those of a wind turbine blade was studied in the laboratory using the known pulsed thermography technique. This allowed the test of numerical methods of image processing created for the inspection of wind

turbines. This numerical method is intended to allow the comparison of the blades of a wind turbine between them to detect defects. Finally, moving blades were observed by infrared camera in a wind farm.

## 1 INTRODUCTION

Wind turbines are exposed to harsh environmental conditions day in and day out. The constant exposure to wind, rain, and temperature fluctuations can take a toll on their structural integrity. Even minor defects, if left unaddressed, can lead to catastrophic failures, expensive repairs, and, most concerning, a drop-in energy production efficiency. Traditional methods of inspecting wind turbines are often costly, time-consuming, and reliant on physical inspections, which can be both dangerous and logistically challenging given the towering heights of these machines.

Multiple research teams have investigated the possibility of using passive infrared thermography to inspect turbine blades. Among them, the authors of article [1] mostly focused on the development of a numerical model, with a section presenting thermograms of a moving wind turbine blade. The team from article [2] focused on the inspection of a blade sample at ground level. The team from article [4] show that infrared thermography can enable the detection of blade surface defects. Despite this, few articles have shown the results of the inspection of the blades of active wind turbines using passive thermography.

It would theoretically be possible to use active thermography to inspect wind turbine blade in-situ. The researchers of article [3] developed a drone-mounted thermal excitation source that, when combined with an onboard infrared camera, could be used to inspect wind turbine blades. However, this method would be limited to static blades, limiting its potential.

By utilizing thermal cameras on or near wind turbines, we gain the ability to assess their condition in real-time, without the need for human intervention at precarious heights. Thermal images provide a unique and invaluable perspective, revealing the thermal signatures of potential defects or stress points within the turbine's structure. However, this newfound wealth of data brings its own challenges.

The thermal cameras dedicated to wind turbines generate a continuous stream of thermal images, creating a data volume that is not only impractical but often impossible to process in real-time. This is where our innovative Python-based application steps in, offering a streamlined approach to this monumental challenge. By intelligently selecting which frames to process, we alleviate the computational burden and enable timely, automated defect detection.

The goal of the study was to begin developing a new methodology for the inspections of defects in wind turbine blades by infrared thermography. The article is divided as follows: The first part was to perform a Finite element modeling simulation of the research problem on the COMSOL software. The geometry of the wind turbine blade and the physics were simplified compared to the real-life situation. In the second part, air gaps at multiple depths were modelized inside the blade’s structure to simulate the impact of defects on the temperature distribution at the blade's surface. Experiments were performed in our laboratory. The goal was to test the algorithm developed for the inspection of wind turbines in-Situ. The sample used had

a composition similar to that of a wind turbine blade. The third part of the experiment were the field tests. We were able to go to a wind farm in Southern Quebec for a day at the end of April 2023. Selected wind turbines were observed with the infrared camera for short interval of times. The algorithm was used on some of the collected thermogram sequences. The analysis of the results show that our new methodology has potential but needs multiple refinements before being used in an industrial setting.

## 2 NUMERICAL MODELING AND FEM SIMULATIONS

For the modeling and multiphysics simulation of the problem by finite elements, we chose to use version 6.1 of the COMSOL software available in our laboratory.

The aim of the numerical simulation was to determine whether it was possible to detect delamination in a moving, solar-heated wind turbine blade. To this end, a model of the surface of a wind turbine blade with simplified geometry was created. This geometry is based on the numerical model presented in [1]. The physical and thermal properties of the materials in the model are also taken from the same article.

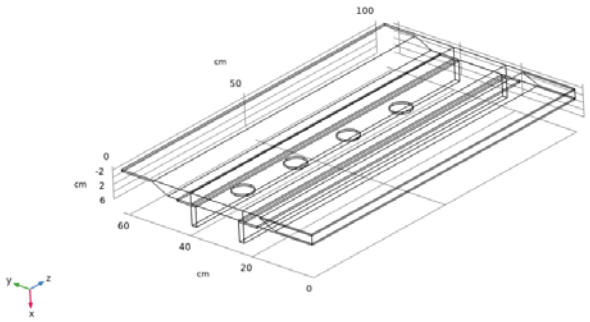


**Figure 1**: Geometry of the wind turbine sample simulated with COMSOL.

Four circular defects, or cavities, have been included in the GFRP section of the model. These four inclusions all have a diameter of 3 cm, a thickness of 0.5 cm and are located at respective depths of 0.5, 1.0, 1.5 and 2 cm below the blade surface. These cavities simulate delaminations located at different depths beneath the blade surface.

The emissivity of the blade surface is assumed to be 0.95. The external convection coefficient, at the blade surface, is 60 W/mK, to represent the fact that the rotating blade is exposed to forced convection. The other surfaces, representing the interior of the blade, are subject to a convection coefficient of 2.5 W m/K and are assumed to emit no radiation.

The ambient properties of the numerical model were based on data from the Beauceville weather station in Quebec. Solar loading (heating) of the blade surface is simulated directly by COMSOL, using an option that simulates solar radiation as a function of simulation time and geographical location. The position of the sun and its intensity are calculated directly by the software as the simulated time progresses. The sun's position is that observed in Montreal, Canada. The blade has been oriented so that its surface is in a vertical position, and the normal

of its surface is aligned towards the south, to maximize the intensity of solar radiation. The start of the simulation was defined as April 20, 2023, close to the date of the field measurements.

The simulation was conducted using a finer mesh. The duration of the simulated time was 5 days, with a time step of 30 minutes. The duration was chosen so that the blade surface temperature would not depend on the initial conditions, which were arbitrarily determined.

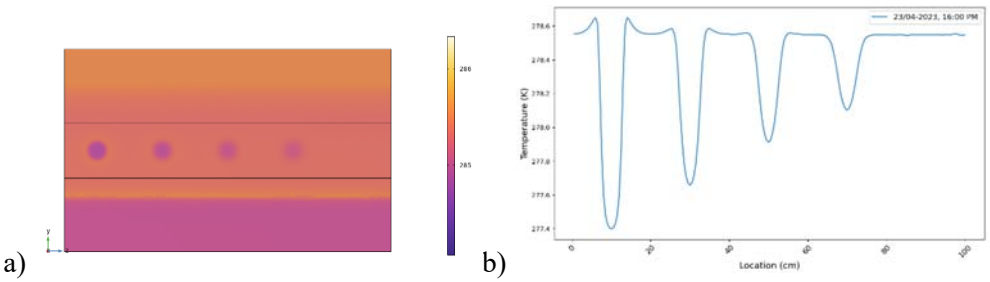


**Figure 2:** a) Surface temperature of the wind turbine blade 35 hours after the start of the simulation. b) Surface temperature of the wind turbine blade vs location 35 hours after the start of the simulation.

Figure 2 shows, at the simulation time of 4 PM on April 23, the surface temperature of the entire sample and the surface temperature along a line intersecting the center of every defect. It is clearly visible on both subfigures that the presence of defect in the sample's subsurface create temperature contrasts visible on its surface. Both subfigures also show, as expected, that at a given time, the temperature contrast created by a defect is larger when the defect is closer to the surface. From left to right on both figures, the temperature contrasts are created by defects located at 0.5, 1.0, 1.5 and 2.0 cm beneath the sample's surface. The contrast created by the defect at a depth of 0.5 cm is about two times greater than the contrast created by a 2 cm-deep defect.

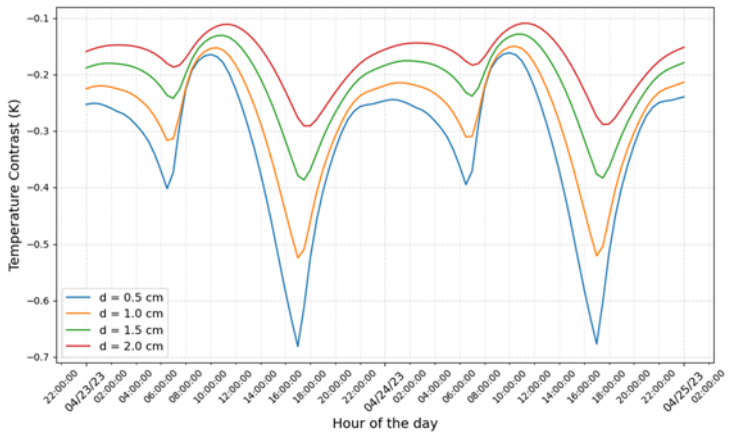


**Figure 3:** Effective Temperature contrast generated by each defect according to the time of the day. The legend indicates the depth (d) of each defect beneath the surface, and the corresponding line.

Figure 3 shows show the effective temperature contrast produced by each defect varies according to the time of the day. The temperature contrast is defined as half the difference between the temperature of sections where there are no defects and the minimum temperature of "troughs" caused by defects, such as those visible in figure 2 b). In fact, the maximum temperature contrast is only observable over a small area, so we consider the effective contrast to be half of the maximum contrast.

The results shown in figure 3 correspond to the third and fourth days of the simulation, excluding the first two days. This ensures that the surface temperature in the analyzed period is not affected by the arbitrary initial conditions and has entered a permanent regime.

It is possible to see that the effective temperature contrast varies in a cyclical pattern, caused by the day-night cycle, with slight variations occurring due to the fluctuating air temperature. As expected, the absolute temperature contrast for the deepest defect, at d = 2.0 cm, reaches a maximum of 0.3 K. Another important aspect to notice is that the absolute effective temperature contrast reaches a local minimum point and local maximum point twice in a day. Those local minima and maxima are reached around the same hours in both cycles analyzed in figure 4. The first local minimum occurs between 1:00 and 2:00, the second local minimum occurs between 11:00 and 12:00. The first local maximum occurs between 5:00 and 6:00, and the second local maxima occurs at approximately 17:00. The second local maximum point is the largest one, making it theoretically the best time to observe the temperature contrasts created by subsurface defects. It is also possible to see that, depending on the subsurface depth, the local minima and maxima are reached at slightly different times, but the effect of subsurface defect depth is small compared to the overarching effect of the day-night cycle.

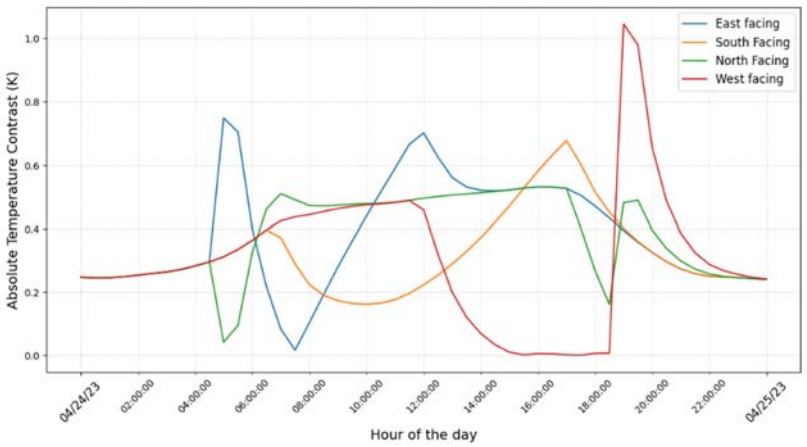


**Figure 4:** Absolute effective temperature contrast by each defect by orientation, in relation to the time of the day.

Other simulations have been made with the sample's surface oriented in other directions, e.g. towards the west, the east and the north. The results show that larger temperature contrasts are achieved at some moments of the day, like in figure 4, but these moments are not the same. For example, in the eastward orientation, the highest contrast in achieved at around 5:00, soon

after sunrise, and for the westward orientation, the highest contrast is achieved at around 19:00, after sunset. These are the moments when the sun rays are the closest to being perpendicular to the sample's surface. It should also be noted that in the early hours after sunset, at around 19:00, a significant temperature contrast can be observed on all orientations. This is in-line with previous studies done on concrete samples exposed to solar radiation [5].

In a real-life scenario, the wind turbine blade will not always have the same orientation, so the optimal moment may not be determined trivially. Future works may try to simulate the effect of a variation of the orientation on the results, based on prevailing wind patterns, for example.

## 3 LAB EXPERIMENT

Experiments were performed in our laboratory [6]. The goal was to test the algorithm developed for the inspection of wind turbines in-Situ. The sample used had a composition similar to that of a wind turbine blade.

Using an infrared imaging method, more specifically the pulsed thermography (PT) technique. The principle was to place a sample on a stand, to heat it with specific flashes and at the same time to visualize the evolution of the temperature within the sample as a function of time with an infrared camera. Since it was not possible to obtain a wind turbine blade sample (due to their size), a sample with a composition similar to that of a wind turbine blade was used in the lab experiment. The images collected during these tests could be recovered and integrated into an image processing process using Python. This is the first step in automating the inspection process in the industry to easily and quickly identify defects within a wind turbine blade..

The experiment was based on the principle of PT. The protocol was therefore to place the sample in front of two heated light flashes, each dissipating an energy of 6.2kJ over 2ms. At the same time, a FLIR X8500 infrared camera equipped with a 50 mm lens filmed the temperature evolution inside the sample to visualize its internal structure. A first sequence was recorded using a frame rate of 50 Hz for 1000 frames in total, and another sequence was recorded using a frame rate of 17 Hz and 1000 frames in total.

**Figure 5:** Front view of the sample used in the lab experiment. The vertical red line on the left side indicates a line defect beneath the surface.

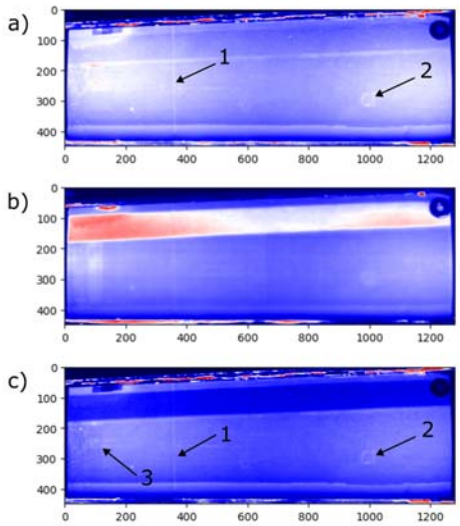


**Figure 6:** a) View of channel 1, average of frames b) View of channel 2, average of frames 90 to 95. C) View of channel 1 – channel 2. The observed defects are numbered from 1 to 3

The thermograms sequences were analyzed using the algorithm described in section 4. In subfigure 6 a), we can see that temperature contrasts are taking shape in a vertical line in the left-hand side of the sample, identified as defect number 1, and a small circle in the right-hand side of the sample, identified as defect number 2. Both temperature contrasts correspond to defects in the sample already known beforehand, shown as markings on the sample visible in figure 5. In subfigure b), those temperature contrasts have mostly disappeared, as the sample cooled down after a longer period. Subfigure c) shows the subtraction of the channels viewed in subfigures a) and b). We see both the vertical line and circle shapes of temperature contrasts visible in subfigure a) in addition to an oblong-shaped temperature contrast in the left-hand side of the sample, identified as defect number 3. This oblong shape corresponds to another defect that was already known to be present in the sample. This oblong-shaped temperature contrast is harder to see in subfigure a) than subfigure c), which show the potential of the algorithm in making the detection of defects in thermograms easier.

Several difficulties were encountered which may have affected the results obtained. The heating used in the experiment seems inadequate in comparison with the modeling part. Here, the heating is very rapid and very powerful. The sun heats the sample continuously over a long period. As far as the modeling of the experiment is concerned, it would have been useful to model the blade sample with the heating conditions used and an appropriate geometry to make a coherent comparison. Unfortunately, many of the sample's characteristics, such as its internal structure, were impossible to obtain without destroying the available blade sample.

## 4 NUMERICAL ALGORITHM

The thermal cameras attached to wind turbines generate a continuous stream of thermal images, creating a data volume that is not only impractical but often impossible to process in

real-time. This is where our innovative Python-based application steps in, offering a streamlined approach to this monumental challenge. By selecting which frames to process, we alleviate the computational burden and enable timely, automated defect detection.

Step 1- Input Video Selection: When the user selects a video file captured by a thermal camera, our application begins by reading and extracting the raw data. The video is typically stored as a series of individual frames, in TIFF format, each representing a thermal image snapshot.

Step 2 -Frame Selection and Channel Assignment: The application presents the user with a comprehensive view of all the frames contained within the video. At this stage, the user is given the freedom to select specific frames they want to analyze for thermal defects. These selected frames can be organized into three distinct channels. This channel assignment allows the user to categorize frames for comparative analysis, which is especially useful for identifying defects in different scenarios or contexts.

Step 3 - Averaging Within Channels: Within each channel, the application performs frame averaging. For frames assigned to Channel 1, for example, all the images are averaged together. This averaging process calculates the mean thermal signature within the selected channel. This step is repeated for each of the three channels.

Step 4 - Channel Comparison: Now that we have averaged thermal signatures for each channel, we proceed to compare the channels individually. This comparison aims to reveal temperature variations and thermal anomalies between the channels. To achieve this, the application computes the differences between the channels pair wise:

Channel 1 vs. Channel 2 (1-2): The difference between the mean thermal signature of frames in Channel 1 and Channel 2 is calculated.

Channel 1 vs. Channel 3 (1-3): Similarly, the difference between the mean thermal signature of frames in Channel 1 and Channel 3 is computed.

Channel 2 vs. Channel 3 (2-3): Finally, the application calculates the difference between the mean thermal signature of frames in Channel 2 and Channel 3.

By comparing these channel pairs, the application provides insight into thermal variations and defect anomalies specific to each channel. Users can easily identify discrepancies in thermal patterns, allowing for the efficient detection of defects or irregularities that might otherwise go unnoticed.

In summary, our Python-based application takes raw thermal data from a video, lets users organize frames into distinct channels, averages thermal signatures within those channels, and computes differences between the channels. This method provides an effective way to detect thermal defects and temperature variations in the analyzed thermal images, ultimately contributing to the reliability and safety of the equipment under inspection.

It is important to state that this Python-based thermal defect detection application is an ongoing project. While it shows promising results in efficiently processing thermal images for wind turbine maintenance, we continue to fine-tune and enhance its capabilities. Our commitment to improvement means that we are actively exploring new features, refining existing algorithms, and seeking feedback to make this tool even more effective.

## 5 FIELD EXPERIMENT

The aim of this part is to visualize a static or moving wind turbine blade with an infrared camera in the field, to spot any defects. The heat source is the sun, which heats the wind turbine blades in a variable way depending on the time of year and when the measurement is taken.

Throughout the day, the temperature was around 10°C. The morning was cloudy and the afternoon was sunny. The camera used was a cooled FLIR model A6701 MWIR, with a 50 mm lens. It was mounted on a tripod and powered by a car battery connected to a power inverter. The sequences were recorded at a frame rate of 60 Hz and an integration time of 4 ms. The camera was located at a variable distance from the wind turbines under study, but it was usually about 200 m. This large distance is necessary to view the blades with an angle that is not too far from their normal. The main area of the blades under study is close to the hub, at a height of 90 m from the ground. The distance between the camera and the observed zone was therefore 220 m. The 50mm lens, combined with the 640 x 512 resolution of the camera, means that the resolution achieved was only 6cm/pixel. This low resolution prevents the detection of small defects and other limited inhomogeneities in wind turbine blades. However, it was believed that the resolution is sufficient for an initial inspection of wind turbine blades using infrared thermography, to test the algorithm and possibly detect large defects such as those due to lighting (a typical issue at that location).

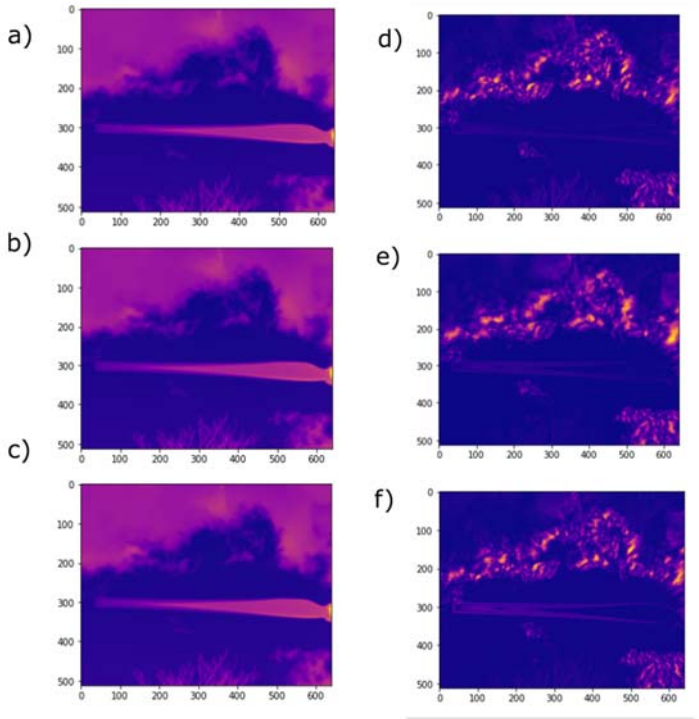

**Figure 7:** Thermograms produced by our algorithm from a recording of the blades of one wind turbine. a) View of channel 1, b) View of channel 2, c) View of channel 3, d) Channel 1 – Channel 2, e) Channel 1 – Channel 3, f) Channel 2 – Channel 3

In figure 7, we can see the results of one of the thermograms sequences acquired during our field experiments. Each subfigure from a) to c) shows the resulting image of channel 1 to 3 of our algorithm, respectively. Each channel corresponds to one of the three blades of the wind turbine. For each channel, 3 consecutive frames were averaged to obtain a single thermogram. Subfigures d) to f) show the result of subtracting each channel against the other two channels.

The results from subfigures d) to f) don't show any error that could be identified with the tools in hand by comparing these frames. We can see that the tips of the blades aren't well-defined, which is a consequence of averaging three consecutive frames for each channel. This shows that our algorithm in its current form cannot be used to detect defects in the tip of the blades, but this could be corrected in future versions. For example, the frames to be averaged for each channel could be extracted from consecutive rotations of the blades, instead of consecutive frames, removing the superposition effect seen at the tips of the blades. However, this limitation of the algorithm should not prevent us from seeing defects near the base of the blades, but no abnormal temperature contrast can be seen in the analyzed frames.

This apparent absence of defects could be a sign that the wind turbines blades have no internal defects that could cause a temperature contrast to be visible in the thermograms. This could be the case as the analyzed wind turbines are recent (circa 2019). However, it is possible that defects could have been detected if some experimental problems were resolved. These experimental problems are summarized in table 1.

| Type of problem | Description |
|---|---|
| Wind turbine blade movement | The orientation of the wind turbine blades is controlled by the wind direction and not by the position of the sun, so if the wind turbine head rotates during the observation period, this prevents images from successive rotations from being directly compared against each other. |
| Observation time | According to the modelling, the best time to observe defects with an infrared camera seems to be around 6 pm. This is because the wind turbine blades have had time to warm up throughout the day thanks to the sun, and suddenly undergo a temperature change due to sunset. In our case, the turbines were pointing west and observed in the early afternoon at about 14:00, which is not the most optimal time, especially for west-facing blades, as figure 4 shows. |
| Lens | For financial reasons, the lens used on the infrared camera has a focal length of 50 mm. As mentioned above, this results in a rather poor resolution of around 6cm/pixel. This makes it difficult to observe defects accurately at such a resolution. Making measurements with a 100 mm or 200 mm focal length lens would undoubtedly yield better results (this is planned). |
| Integration time | The integration time for each thermogram was set at 4 ms to reduce the noise present in each image. However, it was found that parts of wind turbine blades reached saturated values when reflecting sunlight. Also, in case of rapid blade turbine movement, they might be blurred in the images, especially near the tip. |

**Table 1:** Description of problems encountered in field experiments

In summary, our field experiments showed that multiple changes would be necessary to obtain better results. Chief among them would be to get a lens with a higher focal lens, to have a better resolution. A better planning of the experimental parameters, including the time of observation and the acquisition settings, would also be of great importance. Finally, the algorithm could be improved in multiple ways to allow a better analysis of the thermogram sequences, like adding frames from subsequent rotations rather than consecutive frames.

## 6 CONCLUSION

In this article, we present a method that would enable operators to identify defects within a wind turbine blade using infrared imaging technologies. An image processing algorithm has been developed to process the data collected in the field. Beforehand, the algorithm was tested and validated on experimental tests in the laboratory. Finally, a multiphysics model of the problem was set up for comparison and validation purposes. In particular, it was used to find the right time of day and blade orientation for optimal experimental measurements in the field. To improve our approach, it would be important to resolve the problems cited and automate the algorithm and image processing for defect detection.

## AKNOWLEDGMENTS

The results we have presented in this article would not have been possible without the support of several partners. First, we would like to thank the staff of Laval University, especially Clemente Ibarra Castanedo, for having supervised our experiments. We would also like to thank M. Marc-Antoine Landry, assistant facility manager, and the staff of the Mont Saint-Marguerite wind farm (Pattern Energy) near Quebec City for allowing us to enter their site for the field experiments. Finally we acknowledge the support of the following programs: NSERC *Discovery grants*, *Canada Research Chair* and the *Coopération Québec-Colombie 2022-2024* program from Ministère des Relations internationales et de la Francophonie of Québec.

## BIBLIOGRAPHY

[1] Stamm, M., & Krankenhagen, R. (2022, May). Weather-dependent passive thermography of unheated wind turbine blades. In *Thermosense: Thermal Infrared Applications XLIV* (Vol. 12109, pp. 107-114). SPIE.
[2] Sanati, H., Wood, D., & Sun, Q. (2018). Condition monitoring of wind turbine blades using active and passive thermography. Applied Sciences, 8(10), 2004.
[3] Deane, S., Avdelidis, N. P., Ibarra-Castanedo, C., Williamson, A. A., Withers, S., Zolotas, A., ... & Tsourdos, A. (2023). Development of a thermal excitation source used in an active thermographic UAV platform. *Quantitative InfraRed Thermography Journal*, *20*(4), 198-229.
[4] Traphan, D., Herráez, I., Meinlschmidt, P., Schlüter, F., Peinke, J., & Gülker, G. (2018). Remote surface damage detection on rotor blades of operating wind turbines by means of infrared thermography. Wind energy science, 3(2), 639-650.
[5] Pozzer, S., López, F., Dalla Rosa, F., Pravia, Z. M. C., & Maldague, X. (2022, May). Use of advanced thermographic signal processing techniques to improve the subsurface damage detection in concrete columns under varying solar exposure. In *Thermosense: Thermal Infrared Applications XLIV*. SPIE.
[6] Maldague, X. (2000). Applications of infrared thermography in nondestructive evaluation. Trends in optical nondestructive testing, 591-609.